CrystEngComm

COMMUNICATION

View Article Online
View Journal

Cite this: DOI: 10.1039/c7ce00094d

Received 13th January 2017,
Accepted 17th February 2017

DOI: 10.1039/c7ce00094d

rsc.li/crystengcomm

An *in situ* investigation of the water-induced phase transformation of UTSA-74 to MOF-74(Zn)†

Bart Bueken,[a] Helge Reinsch,[b] Niclas Heidenreich,[b] Annelies Vandekerkhove,[a] Frederik Vermoortele,[a] Christine E. A. Kirschhock,[a] Norbert Stock,[b] Dirk De Vos[a] and Rob Ameloot*[a]

We report the water-induced transformation of the [Zn_2(dobdc)] (dobdc = 2,5-dioxidobenzene-1,4-dicarboxylate) metal–organic framework UTSA-74 to its polymorph MOF-74(Zn), contrary to a previous report on the stability of UTSA-74 under such conditions. This dissolution–recrystallization process was investigated using time-resolved *in situ* X-ray diffraction and kinetically analyzed using the Gualtieri crystallization model.

The outcome of metal–organic framework (MOF) syntheses remains hard to predict *a priori*.[1] In some reaction systems, simple variations in synthesis temperature or time can lead to the formation of different congeners or even polymorphs from the same synthesis mixture. Well-known examples include cobalt succinates,[2,3] lithium tartrates,[4,5] and the aluminium/chromium terephthalates MIL-101 and MIL-53.[6] Recently, this series of examples was expanded with UTSA-74 (ref. 7) and MOF-74 (Fig. 1),[8] the latter also known as CPO-27(Zn),[9,10] two polymorphs of [Zn_2(dobdc)($G)_2$] (dobdc = 2,5-dioxido-1,4-benzenedicarboxylate; G = coordinated guest). MOF-74(Zn) is a well-studied material, featuring one-dimensional hexagonal channels formed by continuous helical chains of edge-sharing octahedrally coordinated Zn^{2+} nodes, interconnected *via* dobdc^{4-} linkers (Fig. 1a). The coordination sphere around each Zn^{2+} consists of three carboxylate oxygen atoms, two phenolate oxygen atoms and a coordinated guest molecule, which can be removed to yield a square pyramidal ZnO_5 polyhedron with one coordinatively unsaturated site. Due to the very high density of such sites, MOF-74-type frameworks have seen considerable interest in gas storage and separation, most notably for CO_2, H_2, and light hydrocarbons.[11–20] A variety of synthetic strategies have been reported for MOF-74(Zn), including liquid assisted grinding[21] and water-based syntheses relying on stoichiometric amounts of NaOH to deprotonate the H_4dobdc linkers.[22,23] However, most syntheses are based on the originally reported solvothermal synthesis,[8] where H_4dobdc and $Zn(NO_3)_2{\cdot}6H_2O$ are dissolved in *N*,*N*-dimethylformamide (DMF) together with a small amount of water, presumably for solubility reasons, and allowed to react at 105 °C.

Recently, Luo *et al.*[7] found that performing this synthesis at a higher temperature (158 °C) did not lead to the formation of MOF-74(Zn), but rather to a previously unreported polymorph denoted UTSA-74. This structure (Fig. 1b, left) crystallizes in the rhombohedral space group $R\bar{3}c$ and features one-dimensional channels, similar to those of MOF-74(Zn). However, in UTSA-74 these channels are delineated by chains of dobdc^{4-} linkers alternating with discrete Zn^{2+}

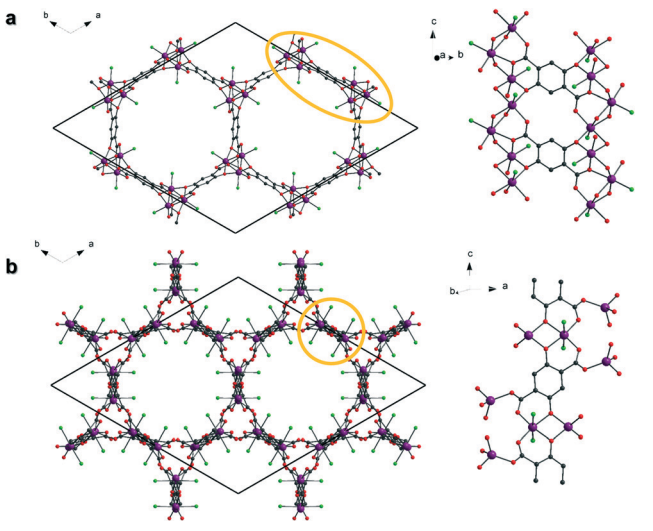

Fig. 1 Structures (left) of MOF-74(Zn) (a) and UTSA-74 (b), as viewed along their *c*-direction. Both frameworks feature significantly different binding motifs between dobdc^{4-} and Zn^{2+}, as indicated by the close-up of the highlighted area (right). Zn = purple; O = red; C = grey; guest = green.

[a] *Centre for Surface Chemistry and Catalysis, Department M^{2}S, KU Leuven, Celestijnenlaan 200F p.o. box 2461, 3001 Leuven, Belgium. E-mail: rob.ameloot@kuleuven.be*
[b] *Institut für Anorganische Chemie, Christian-Albrechts Universität zu Kiel, Max-Eyth Straße 2, D-24118 Kiel, Germany*

† Electronic supplementary information (ESI) available. See DOI: 10.1039/c7ce00094d

dimers (Fig. 1b, right) rather than by the helical ZnO_6-chains found in MOF-74, leading to the novel **fgl** topology. Each dimer in UTSA-74 consists of an edge-sharing pair of a tetrahedrally and an octahedrally coordinated Zn^{2+} ion, with two phenolate μ-O atoms forming the shared vertices of these polyhedra. The coordination environment of the tetrahedral Zn^{2+} ions is completed by two carboxylate oxygen atoms originating from $dobdc^{4-}$ linkers in neighbouring chains. Similarly, the equatorial plane of the octahedral Zn^{2+} ion, containing the phenolate oxygen atoms, is completed by two carboxylate oxygen atoms of the $dobdc^{4-}$ linkers in the same chain as the dimer. The *trans* apical positions are occupied by guest molecules that line the pore walls. Interestingly, the presence of two coordinatively unsaturated sites on a single Zn^{2+} ion after guest removal results in very different sorption properties for UTSA-74 compared to MOF-74(Zn), with superior performance in the separation of C_2H_2 from CO_2.[7]

During our own synthetic efforts in the Zn^{2+}/H_4dobdc system, we observed that large (up to 300 μm), hexagonal crystals of UTSA-74 (Fig. S1†) can also be prepared *via* an alternative synthesis, by reacting $Zn(CH_3COO)_2{\cdot}2H_2O$ (4.5 mmol) and H_4dobdc (2.5 mmol) in dimethyl sulfoxide (DMSO) at 110 °C for 72 h. The UTSA-74 structure was confirmed by X-ray diffraction of both single crystals and crushed samples (Fig. 2a, Table S1†). Following UTSA-74 synthesis, FTIR and TG analysis indicated the presence of DMSO molecules in the pores, likely occupying the apical sites of the octahedral Zn^{2+} nodes (Fig. S2 and S3†). These guest molecules could be efficiently exchanged by soaking the as-synthesized crystals five times in ethanol at 80 °C overnight. From the nitrogen physisorption isotherm obtained after activation at 150 °C under vacuum for 4 h (Fig. 2b), a Brunauer–Emmett–Teller (BET) specific surface area of 890 $m^2\ g^{-1}$ was calculated, which is comparable to the value obtained by Luo *et al.* (830 $m^2\ g^{-1}$).[7] Likewise, a similar CO_2 uptake of 6.08 mmol g^{-1}, or approximately one CO_2 molecule per Zn^{2+} dimer was measured (Fig. S4†).

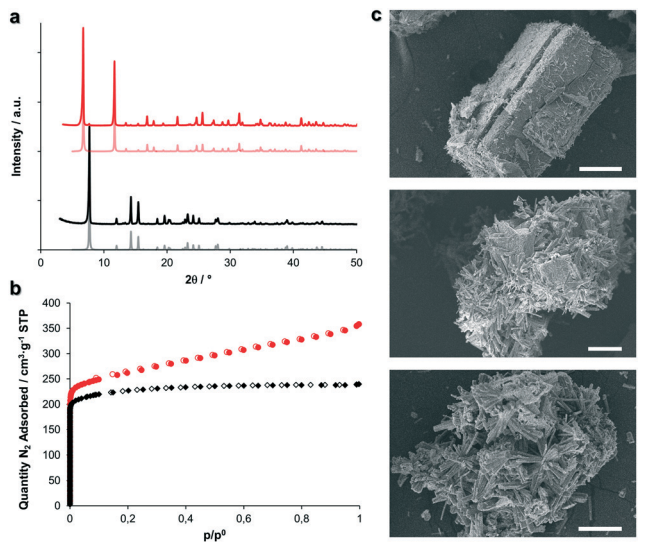

Fig. 2 (a) Powder X-ray diffraction patterns of UTSA-74 (black) and MOF-74(Zn) (red) obtained by recrystallization from UTSA-74 at 110 °C in water. Theoretical diffraction patterns[7,10] presented in grey and pink, respectively. (b) Nitrogen physisorption isotherms (77 K) of UTSA-74 (black diamonds) and MOF-74(Zn) (red circles) obtained by recrystallization from UTSA-74 at 110 °C in water. Full symbols = adsorption branch; open symbols = desorption branch. (c) SEM micrographs of various stages of dissolution–recrystallization of UTSA-74 into MOF-74(Zn) at 50 °C under static conditions. Top: A large UTSA-74 crystal with needle-like MOF-74(Zn) crystals growing onto it (1 h reaction, scale bar = 100 μm); middle & bottom: fragments of UTSA-74 crystals covered with MOF-74(Zn) crystals, after 2 and 4 h reaction time, respectively. Scale bars = 50 μm (see also Fig. S9 and S10†).

The original report on the discovery of UTSA-74 stated stability of the material in organic solvents and water in the pH range 3–10.[7] Surprisingly, while we indeed found UTSA-74 to be stable in various organic solvents (Fig. S5†), in our hands exposure to water, either in liquid form or as a vapour, induced gradual but clear changes in the material's powder X-ray diffraction pattern (Fig. S6 and S7†). In a preliminary static *in situ* experiment at ambient temperature, the reflections of UTSA-74 submerged in water in a sealed glass capillary gradually disappeared over the course of ~7.5 h, with a concomitant appearance and growth of a new set of reflections. The diffraction pattern of the newly obtained phase strikingly matched that of hydrated MOF-74(Zn) (Fig. 2a),[11] indicating a conversion from one [Zn_2(dobdc)] polymorph into another. Upon careful re-examination of the diffraction data of the water stability tests in the original UTSA-74 report,[7] a partial phase transformation to MOF-74(Zn) was also observed, albeit at an apparently slower rate than we found (Fig. S8†).

The MOF-74(Zn) formed by transformation of UTSA-74 shows excellent microporosity (Fig. 2b), with a BET surface area of 986 $m^2\ g^{-1}$, well within the reported range for MOF-74(Zn) samples prepared directly from H_4dobdc and a Zn-salt.[22] Scanning electron micrographs (SEM) recorded at various stages of the transformation process further show the growth of small, needle-like crystals of MOF-74(Zn) nucleated on the surface of the large UTSA-74 single crystals, and the concomitant disintegration of the latter (Fig. 2c, Fig. S9 and S10†). These observations clearly indicate that the phase transformation of UTSA-74 to MOF-74(Zn) occurs not as a single-crystal-to-single-crystal process, but rather *via* a dissolution–recrystallization mechanism.

To gain a deeper insight into the process and the kinetics underlying this transformation, time-resolved *in situ* X-ray diffraction experiments were undertaken at 110 °C and 120 °C at beamline P08 at PETRA III (DESY, Hamburg),[24] using a custom-built *in situ* cell (details in ESI†). In each experiment, 100 mg of ethanol-exchanged UTSA-74 crystals was suspended in 3 ml deionized H_2O and rapidly heated to the desired temperature under stirring. Diffraction data were recorded with a temporal resolution of 30 s, as presented in Fig. 3a and b. The disappearance of UTSA-74 by dissolution ($\alpha_{UTSA\text{-}74}$) and the extent of MOF-74(Zn) crystallization ($\alpha_{MOF\text{-}74}$) were determined by normalizing the intensity of their strongest reflection ($(2\bar{1}0)$ for both phases) against its maximum value, as this can be considered proportional to the concentration of each

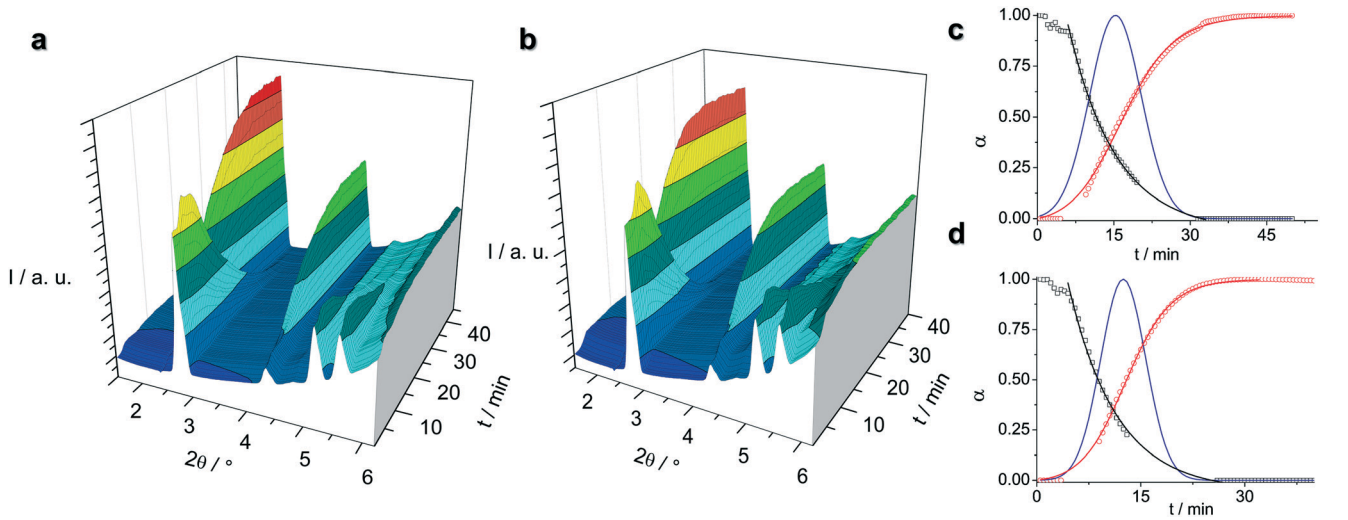

Fig. 3 Time-resolved *in situ* X-ray diffraction data (λ = 0.51662 Å) of the conversion of UTSA-74 to MOF-74(Zn) at 110 °C (a) and 120 °C (b). The initial increase in intensity can be attributed to the heating of the *in situ* cell. Extent of reaction (α) at 110 °C (c) and 120 °C (d) as a function of time, starting after the desired temperature was reached. The dissolution of UTSA-74 (black squares) could be fitted using an exponential decay function (black curves) following an initial stage of slow intensity decrease, while the recrystallization as MOF-74(Zn) (red circles) is described adequately by the Gualtieri model for crystallization (red curves). The blue curves represent the probability of nucleation P_N.

phase. The obtained evolution of $\alpha_{UTSA\text{-}74}$ and $\alpha_{MOF\text{-}74}$ at 110 °C and 120 °C is plotted in Fig. 3c and d, respectively.

At both temperatures, following an initial stage of slow intensity decrease for UTSA-74, a steep decay of $\alpha_{UTSA\text{-}74}$ is observed, which is fitted well by an exponential decay function (Table 1):

$$\alpha_{UTSA\text{-}74} = e^{-((t-t_0)\cdot k_{diss})}$$

The value of t_0, considered as the onset of the exponential regime, was set at 6.5 min and 4.5 min at 110 °C and 120 °C, respectively. The pseudo-first order rate constant for UTSA-74 dissolution (k_{diss}), increases significantly with temperature, adopting values of 0.11(1) min^{-1} (110 °C) and 0.15(3) min^{-1} (120 °C), leading to near-complete disappearance of UTSA-74 after approximately 32 min at 110 °C and 26 min at 120 °C.

The first reflections of MOF-74(Zn) start to appear after 6 min and 5 min at 110 °C and 120 °C, respectively, corresponding more or less to the point at which the dissolution of UTSA-74 accelerates and enters the exponential regime. $\alpha_{MOF\text{-}74}$ subsequently reaches its maximum value after 48 min and 32 min, respectively, at 110 °C and 120 °C. Note that after this time a slow intensity decrease in the MOF-74(Zn) powder pattern can be observed, hinting at decomposition of MOF-74(Zn) in water.[25–28] Kinetic information on MOF-74(Zn) formation was extracted from the data by applying the model developed by Gualtieri, originally to describe the crystallization kinetics of zeolites[29] but frequently applied to *in situ* crystallization studies of MOFs.[5,30–35] The model fits the extent of crystallization, in our case $\alpha_{MOF\text{-}74}$, as a function of crystallization time t:

$$\alpha_{MOF\text{-}74} = \frac{1}{1+\exp\left(-\frac{t-\alpha}{b}\right)} \cdot \left[1-\exp\left(\left(-k_g\right)^n\right)\right]$$

Nucleation and growth are considered as separate processes, and described by different fitting parameters. The parameters a and b relate to nucleation, respectively representing the maximum and variance of the Gaussian probability distribution of the number of formed nuclei P_N as a function of t.

$$P_N = \exp\left(-\frac{(t-a)^2}{2b^2}\right)$$

Hence, the inverse of a can be interpreted as the rate constant for nucleation, k_n, whereas b provides information on the nucleation mechanism. Crystal growth is captured in the rate constant k_g and the parameter n, which relates to the dimension of crystal growth. We set n = 1, based on the needle-like morphology of the formed MOF-74(Zn) crystals (Fig. 2c) and in accordance with the work of El Osta *et al.*[33] on the crystallization of MOF-74(Co) and MOF-74(Ni). In our study, $\alpha_{MOF\text{-}74}$ was fitted well by the Gualtieri model when disregarding the regime where the reflections of MOF-74(Zn) again start losing intensity. The fitted parameters at both investigated temperatures are summarized in Table 1.

Table 1 Fitted parameters for the dissolution of UTSA-74 ($\alpha_{UTSA\text{-}74}$) by an exponential decay function, and for the crystallization of MOF-74(Zn) ($\alpha_{MOF\text{-}74}$) by the Gualtieri model (n = 1)

	110 °C	120 °C
A	1.98(2)	2.12(4)
k_{diss} (min^{-1})	0.11(1)	0.15(1)
a (min)	15.31(29)	12.47(21)
b (min^{-1})	5.06(12)	3.24(6)
k_n (min^{-1})	0.065(2)	0.080(1)
k_g (min^{-1})	0.118(9)	0.206(29)

At both temperatures, nucleation seems to be the rate-limiting process in MOF-74(Zn) formation, with k_n being smaller than k_g, and extends well into the crystallization period, as indicated by the nucleation probability distribution P_N. Furthermore, since $b \leq 15$, nucleation can be interpreted to proceed in a heterogeneous fashion,[29] as also indicated by the SEM micrographs, showing growth of MOF-74(Zn) onto the UTSA-74 crystals. While both nucleation and growth are accelerated by increasing the reaction temperature, this effect is far more pronounced for the latter, with k_g rising from 0.118(9) min^{-1} at 110 °C to 0.206(29) min^{-1} at 120 °C. These values are rather low compared to those extracted from *in situ* data on the crystallization of MOF-74(Co) and MOF-74(Ni) from H_2O/tetrahydrofuran synthesis solutions.[33] The latter study yielded very high values for Co^{2+} (k_g = 0.586(8) min^{-1} and k_n = 0.7174(77) min^{-1} at 100 °C) and moderate for Ni^{2+} (k_g = 0.199(7) min^{-1} and k_n = 0.2500(81) min^{-1} at 110 °C). A similar trend could be observed for the nucleation rate constants k_n. Moreover, k_n was found to be consistently higher than k_g for the syntheses of MOF-74(Co) and MOF-74(Ni), whereas in our case $k_g > k_n$ in both experiments.[33] In spite of the higher expected reactivity of the Zn^{2+} cation, we attribute this discrepancy to the rate-determining dissolution of UTSA-74, limiting the amount of reactants present in solution. The curves of $\alpha_{UTSA\text{-}74}$ and $\alpha_{MOF\text{-}74}$ intersect at a value of $\alpha \approx 0.4$. In case this intersection would have occurred at 0.5, a direct conversion of UTSA-74 to MOF-74 could be assumed. However, at the intersection point only 40% of each phase's maximum amount is observable in dispersion. The remaining non-diffracting matter is present as X-ray amorphous intermediates or dissolved reactants and corresponds to the building blocks available for the formation of MOF-74(Zn).

Following Ostwald's rule of stages,[36] the conversion of UTSA-74 into MOF-74(Zn) should form a thermodynamic series. Indeed, an increasing degree of condensation of the inorganic nodes in MOFs has previously been associated with the formation of thermodynamically more stable phases at increasing temperatures.[2,37] When comparing UTSA-74 and MOF-74(Zn), the conversion of discrete Zn^{2+} dimers into one-dimensional infinite chains leads to an increase in the number of Zn^{2+}-linker bonds from four to five, achieving a hydrolytically more stable coordination environment. This is reminiscent of the water-induced transformation of MOF-5(Zn) to MOF-69c,[38,39] where conversion of discrete $[Zn_4O(COO)_6]$ clusters to infinite chains is also accompanied by an increase in average Zn^{2+} coordination number, from 4 to 4.67. In our synthesis, DMSO might play a unique role in stabilizing the dimeric Zn^{2+} units, and thus steering the synthesis to UTSA-74 rather than MOF-74(Zn). While a detailed investigation into the thermodynamics of the $[Zn_2(dobdc)]$ system is beyond the scope of this report, the observation that the more condensed MOF-74(Zn) is the thermodynamically favoured phase seems to be contradicted by the UTSA-74 synthesis reported by Luo *et al.*, which operates at higher temperatures. However, a similar effect has been observed in other polymorphous hybrid materials,[5,40,41] and there was attributed to vibrational entropic effects (*i.e.* large thermal displacements of lattice atoms), which at high synthesis temperatures played a determining role in stabilizing the metastable phase of higher enthalpy.

Conclusions

A new preparative route towards UTSA-74 was established, employing DMSO as the solvent. In contrast to previous findings, UTSA-74 was found to transform to its polymorph MOF-74(Zn) by hydrolysis. These observations suggest that the latter is the thermodynamically preferred phase under the transformation conditions. This dissolution-recrystallization process was monitored by *in situ* X-ray diffraction and kinetically analyzed using the Gualtieri model.

Acknowledgements

B. B., D. D. V. and R. A. acknowledge funding from the Research Foundation – Flanders (FWO) (post-doctoral grant). R. A. is grateful to KU Leuven for BOF-START funding. The authors thank and acknowledge the assistance of J. Jacobs and L. Van Meervelt (single crystal X-ray diffraction), M. Köppen (software), S. Smolders (SEM), I. Stassen (N_2 physisorption) and M. Aubrey and J. Long (CO_2 sorption). This work has been supported by the MATsynCELL project through the Röntgen-Ångström Cluster, supported by the Swedish Research Council and the German Federal Ministry of Education and Research (BMBF). Parts of this research were carried out at the light source PETRA III at DESY, a member of the Helmholtz Association (HGF). We would like to thank Jörg Strempfer and Uta Ruett for assistance in using beamlines P08 and P09.

References

1 M. Goesten, F. Kapteijn and J. Gascon, *CrystEngComm*, 2013, **15**, 9249–9257.
2 P. M. Forster, A. R. Burbank, C. Livage, G. Férey and A. K. Cheetham, *Chem. Commun.*, 2004, 368–369.
3 P. M. Forster, N. Stock and A. K. Cheetham, *Angew. Chem., Int. Ed.*, 2005, **44**, 7608–7611.
4 H. H.-M. Yeung and A. K. Cheetham, *Dalton Trans.*, 2014, **43**, 95–102.
5 H. H.-M. Yeung, Y. Wu, S. Henke, A. K. Cheetham, D. O'Hare and R. I. Walton, *Angew. Chem.*, 2016, **128**, 2052–2056.
6 N. A. Khan and S. H. Jhung, *Cryst. Growth Des.*, 2010, **10**, 1860–1865.
7 F. Luo, C. Yan, L. Dang, R. Krishna, W. Zhou, H. Wu, X. Dong, Y. Han, T.-L. Hu, M. O'Keeffe, L. Wang, M. Luo, R.-B. Lin and B. Chen, *J. Am. Chem. Soc.*, 2016, **138**, 5678–5684.
8 N. L. Rosi, J. Kim, M. Eddaoudi, B. Chen, M. O'Keeffe and O. M. Yaghi, *J. Am. Chem. Soc.*, 2005, **127**, 1504–1518.
9 P. D. C. Dietzel, Y. Morita, R. Blom and H. Fjellvåg, *Angew. Chem.*, 2005, **117**, 6512–6516.
10 P. D. C. Dietzel, R. E. Johnsen, R. Blom and H. Fjellvåg, *Chem. – Eur. J.*, 2008, **14**, 2389–2397.

11 S. R. Caskey, A. G. Wong-Foy and A. J. Matzger, *J. Am. Chem. Soc.*, 2008, **130**, 10870–10871.
12 S. Xiang, W. Zhou, Z. Zhang, M. A. Green, Y. Liu and B. Chen, *Angew. Chem., Int. Ed.*, 2010, **49**, 4615–4618.
13 E. D. Bloch, W. L. Queen, R. Krishna, J. M. Zadrozny, C. M. Brown and J. R. Long, *Science*, 2012, **335**, 1606–1610.
14 Y.-S. Bae, C. Y. Lee, K. C. Kim, O. K. Farha, P. Nickias, J. T. Hupp, S. T. Nguyen and R. Q. Snurr, *Angew. Chem., Int. Ed.*, 2012, **51**, 1857–1860.
15 E. D. Bloch, L. J. Murray, W. L. Queen, S. Chavan, S. N. Maximoff, J. P. Bigi, R. Krishna, V. K. Peterson, F. Grandjean, G. J. Long, B. Smit, S. Bordiga, C. M. Brown and J. R. Long, *J. Am. Chem. Soc.*, 2011, **133**, 14814–14822.
16 E. D. Bloch, M. R. Hudson, J. A. Mason, S. Chavan, V. Crocellà, J. D. Howe, K. Lee, A. L. Dzubak, W. L. Queen, J. M. Zadrozny, S. J. Geier, L.-C. Lin, L. Gagliardi, B. Smit, J. B. Neaton, S. Bordiga, C. M. Brown and J. R. Long, *J. Am. Chem. Soc.*, 2014, **136**, 10752–10761.
17 W. L. Queen, M. R. Hudson, E. D. Bloch, J. A. Mason, M. I. Gonzalez, J. S. Lee, D. Gygi, J. D. Howe, K. Lee, T. A. Darwish, M. James, V. K. Peterson, S. J. Teat, B. Smit, J. B. Neaton, J. R. Long and C. M. Brown, *Chem. Sci.*, 2014, **5**, 4569–4581.
18 D. Gygi, E. D. Bloch, J. A. Mason, M. R. Hudson, M. I. Gonzalez, R. L. Siegelman, T. A. Darwish, W. L. Queen, C. M. Brown and J. R. Long, *Chem. Mater.*, 2016, **28**, 1128–1138.
19 T. M. McDonald, W. R. Lee, J. A. Mason, B. M. Wiers, C. S. Hong and J. R. Long, *J. Am. Chem. Soc.*, 2012, **134**, 7056–7065.
20 T. M. McDonald, J. A. Mason, X. Kong, E. D. Bloch, D. Gygi, A. Dani, V. Crocellà, F. Giordanino, S. O. Odoh, W. S. Drisdell, B. Vlaisavljevich, A. L. Dzubak, R. Poloni, S. K. Schnell, N. Planas, K. Lee, T. Pascal, L. F. Wan, D. Prendergast, J. B. Neaton, B. Smit, J. B. Kortright, L. Gagliardi, S. Bordiga, J. A. Reimer and J. R. Long, *Nature*, 2015, **519**, 303–308.
21 P. A. Julien, K. Užarević, A. D. Katsenis, S. A. J. Kimber, T. Wang, O. K. Farha, Y. Zhang, J. Casaban, L. S. Germann, M. Etter, R. E. Dinnebier, S. L. James, I. Halasz and T. Friščić, *J. Am. Chem. Soc.*, 2016, **138**, 2929–2932.
22 L. Garzón-Tovar, A. Carné-Sánchez, C. Carbonell, I. Imaz and D. Maspoch, *J. Mater. Chem. A*, 2015, **3**, 20819–20826.
23 M. Sánchez-Sánchez, N. Getachew, K. Díaz, M. Díaz-García, Y. Chebude and I. Díaz, *Green Chem.*, 2015, **17**, 1500–1509.
24 O. H. Seeck, C. Deiter, K. Pflaum, F. Bertam, A. Beerlink, H. Franz, J. Horbach, H. Schulte-Schrepping, B. M. Murphy, M. Greve and O. Magnussen, *J. Synchrotron Radiat.*, 2012, **19**, 30–38.
25 S. S. Han, S.-H. Choi and A. C. T. van Duin, *Chem. Commun.*, 2010, **46**, 5713.
26 A. C. Kizzie, A. G. Wong-Foy and A. J. Matzger, *Langmuir*, 2011, **27**, 6368–6373.
27 N. C. Burtch, H. Jasuja and K. S. Walton, *Chem. Rev.*, 2014, **114**, 10575–10612.
28 K. Tan, S. Zuluaga, Q. Gong, P. Canepa, H. Wang, J. Li, Y. J. Chabal and T. Thonhauser, *Chem. Mater.*, 2014, **26**, 6886–6895.
29 A. F. Gualtieri, *Phys. Chem. Miner.*, 2001, **28**, 719–728.
30 T. Ahnfeldt, J. Moellmer, V. Guillerm, R. Staudt, C. Serre and N. Stock, *Chem. – Eur. J.*, 2011, **17**, 6462–6468.
31 F. Millange, R. El Osta, M. E. Medina and R. I. Walton, *CrystEngComm*, 2011, **13**, 103–108.
32 J. Cravillon, C. A. Schröder, H. Bux, A. Rothkirch, J. Caro and M. Wiebcke, *CrystEngComm*, 2012, **14**, 492.
33 R. El Osta, M. Feyand, N. Stock, F. Millange and R. I. Walton, *Powder Diffr.*, 2013, **28**, S256–S275.
34 F. Ragon, P. Horcajada, H. Chevreau, Y. K. Hwang, U.-H. Lee, S. R. Miller, T. Devic, J.-S. Chang and C. Serre, *Inorg. Chem.*, 2014, **53**, 2491–2500.
35 G. Zahn, P. Zerner, J. Lippke, F. L. Kempf, S. Lilienthal, C. A. Schröder, A. M. Schneider and P. Behrens, *CrystEngComm*, 2014, **16**, 9198–9207.
36 W. Ostwald, *Z. Phys. Chem.*, 1897, **22**, 289–330.
37 G. Férey, *Chem. Soc. Rev.*, 2008, **37**, 191–214.
38 S. S. Kaye, A. Dailly, O. M. Yaghi and J. R. Long, *J. Am. Chem. Soc.*, 2007, **129**, 14176–14177.
39 S. Hausdorf, J. Wagler, R. Moβig and F. O. R. L. Mertens, *J. Phys. Chem. A*, 2008, **112**, 7567–7576.
40 G. Kieslich, S. Kumagai, K. T. Butler, T. Okamura, C. H. Hendon, S. Sun, M. Yamashita, A. Walsh and A. K. Cheetham, *Chem. Commun.*, 2015, **51**, 15538–15541.
41 K. T. Butler, K. Svane, G. Kieslich, A. K. Cheetham and A. Walsh, *Phys. Rev. B*, 2016, **94**, 180103.